Waste Management 170 (2023) 103–111

Contents lists available at ScienceDirect

Waste Management

journal homepage: www.elsevier.com/locate/wasman

Research Paper

Fly ash degree of reaction in hypersaline NaCl and $CaCl_2$ brines: Effects of calcium-based additives

Marie Collin [a,b,*], Yu Song [a,c], Dale P. Prentice [a,b], Ross A. Arnold [a,b], Kirk Ellison [d], Dante A. Simonetti [b,e], Mathieu Bauchy [b,c], Gaurav N. Sant [a,b,f,g,*]

[a] Laboratory for the Chemistry of Construction Materials (LC2), Department of Civil and Environmental Engineering, University of California, Los Angeles, CA, USA
[b] Institute for Carbon Management, University of California, Los Angeles, CA, USA
[c] Physics of AmoRphous and Inorganic Solids Laboratory (PARISlab), Department of Civil and Environmental Engineering, University of California, Los Angeles, CA, USA
[d] Electric Power Research Institute, Charlotte, NC 28262, USA
[e] Department of Chemical and Biomolecular Engineering, University of California, Los Angeles, CA, USA
[f] Department of Materials Science and Engineering, University of California, Los Angeles, CA, USA
[g] California Nanosystems Institute (CNSI), University of California, Los Angeles, CA, USA

ARTICLE INFO

Keywords:
Fly ash
Hypersaline brine
Solidification and stabilization
Thermodynamic modeling
Chemical reactivity

ABSTRACT

The pozzolanic reaction of fly ashes with calcium-based additives can be effectively used to solidify and chemically stabilize (S&S process) highly concentrated brines inside a cementitious matrix. However, complex interactions between the fly ash, the additive, and the brine typically affect the phases formed at equilibrium, and the resulting solid capacity to successfully encapsulate the brine and its contaminants. Here, the performances of two types of fly ash (a Class C and Class F fly ash) are assessed when combined with different additives (two types of cement, or lime with and without $NaAlO_2$), and two types of brine (NaCl or $CaCl_2$) over a range of concentrations ($0 \leq [Cl^-] \leq 2$ M). The best performing matrices – i.e., the matrices with the highest Cl-containing phases content – were identified using XRD and TGA. The experimental results were then combined with thermodynamic modeling to dissociate the contribution of the fly ash from that of the additives. All results were implemented in a machine learning model that showed good accuracy at predicting the fly ash degree of reaction, allowing for the robust prediction of extended systems performance when combined with thermodynamic modeling.

1. Introduction and background

Waste management is a growing challenge for all sectors, as there is an increasing demand for more comprehensive control of waste products. As an example, waste streams including (but not limited to) agricultural, industrial, mining, municipal, and power plant waste waters, as well as produced and extracted water, all require specific attention (Borch et al., 2021; Cath et al., 2021a, 2021b; Childress et al., 2021; Giammar et al., 2021). These waste streams (referred to as brine from hereon due to their high salt concentrations) contain high levels of contaminants (0–5 M of total dissolved solids), yet can be safely landfilled, provided that the pollutants – for instance: heavy metals, alkali and alkaline-earth cations, halide anions, etc.– are effectively immobilized in a solid matrix such as a cementitious solid (Fatoba et al., 2015, 2013; Poon et al., 2004; Renew et al., 2016). This type of binder solidifies and stabilizes (S&S) the contaminants within the solid – either as insoluble species (Glasser, 1997), or by incorporation or sorption into the hydrate phases (Gougar et al., 1996; Piekkari et al., 2020) – to prevent mobile aqueous species release into the environment.

Among the various cementitious binders tested, the use of fly ash(es) has been proven to be of great interest (Okoronkwo et al., 2018; Renew et al., 2016). ASTM C618 compliant coal-fired power plant fly ashes – typically classified either as “Class C” or “Class F” fly ash (ASTM C618, 2019, p. 618) – are commonly mixed with a Ca-containing additive. The pozzolanic reaction between the calcium provided by the additive and the fly ash silicate content leads to the formation of calcium-silicate-hydrate (C-S-H) phases (Poon et al., 2003; Wang and Ishida, 2019), as well as a range of hydrated phases of interest for contaminant binding

* Corresponding authors at: Laboratory for the Chemistry of Construction Materials (LC2), Department of Civil and Environmental Engineering, University of California, Los Angeles, CA, USA.
E-mail addresses: mariecollin03@ucla.edu (M. Collin), gsant@ucla.edu (G.N. Sant).

https://doi.org/10.1016/j.wasman.2023.08.002
Received 21 November 2022; Received in revised form 15 July 2023; Accepted 2 August 2023
Available online 8 August 2023

such as Cl-AFm (e.g., Friedel's salt – $Ca_2Al(OH)_6[Cl, OH]\cdot 2H_2O$) for Cl-containing brines. Relevant calcium-based additives include quicklime (CaO), hydrated lime ($Ca(OH)_2$), and/or ordinary portland cement (OPC) (Ellison, 2019). Increasing the Al content in the system – by using for example a calcium aluminate cement (CAC) – could result in the increased formation of AFm phases of interest. Uncertainties remain, however, on the effect such additives might have on the phase assemblage and the fly ash degree of reaction. Additionally, brine composition and concentration typically affect the phase assemblage and the fly ash degree of reaction.(Poon et al., 2004; Collin et al., 2022) As a result, the complex interaction between brine and additive may further affect the capacity of the solid matrix to immobilize the pollutants, which requires investigation. However, while it is important to identify the best performing encapsulation systems, testing multiple systems is very time consuming. Thermodynamic modeling is a fast and useful tool to rapidly assess the performance of encapsulation systems (e.g., pH, brine consumption, phase equilibrium, etc.) (Collin et al., 2022, 2021; Okoronkwo et al., 2018). Thermodynamic modeling is already well established to predict the equilibrium phases forming from cement hydration.(Lothenbach and Winnefeld, 2006; Lothenbach et al., 2008; Damidot et al., 2011; Lothenbach et al., 2019) Similarly, fly ash pozzolanic reaction can already be estimated as a function of time (Glosser et al., 2020; Lothenbach and Winnefeld, 2006), but the current models rely on empirical data gathered in a OPC and water system where the fly ash is a supplementary cementitious material – i.e., a system that is not representative of a brine encapsulation system where the fly ash is the major reactive component. Gathering empirical data for every system of interest presents significant limitations in terms of cost and time, and severely reduces the appeal of thermodynamic modeling. This emphasizes the necessity to develop alternatives methods to estimate the fly ash degree of reaction for an encapsulation system prior to the modeling if thermodynamic modeling is to be used as a predictive tool for future research.

In order to establish a matrix of well-defined encapsulation systems, (1) two types of fly ashes (a Class C and a Class F fly ash), (2) four types of additives (two types of cement, or lime with and without $NaAlO_2$), (3) two types of brines (NaCl or $CaCl_2$), and (4) various brine concentrations (from 0 to 2 M of Cl^-) were investigated. The phase assemblages formed after 10 days of hydration at 50 °C are used to infer the fly ashes degree of reaction by comparison with thermodynamically modelled phase assemblages. The reactivity of the fly ashes is further validated using isothermal calorimetry, highlighting how each system reacts and their subsequent performance in successfully (or not) encapsulating the brine. The experimental and simulated data are then compiled in an artificial neural network-based machine learning model to properly capture the intricate mapping from the complex interaction within the brine/fly ash/additive system, and their effect on the degree of reaction of the fly ash. By taking into account the initial setup composition, the trained model can accurately predict the fly ash degree of reaction and, more importantly, decipher the distinct effect of fly ash/solution composition on reactivity. As a result, future setups can be rapidly and accurately modeled so that the best fly ash and additives mixes can be paired with specific brine compositions and concentrations.

2. Material and methods

2.1. Raw material characterization

A Class C and a Class F fly ash were studied as representative fly ashes. The additives studied include portlandite $Ca(OH)_2$ (purity > 95%) (abbreviated as CH from hereon), a 95 mass % $Ca(OH)_2$ + 5 mass % $NaAlO_2$ (purity 99%) mix (abbreviated as CH-NA from hereon), a type III anhydrous ordinary portland cement (abbreviated as OPC from hereon) and a "ciment fondu" type of low alumina calcium aluminate cement ("Guide to the selection and use of hydraulic cements," 2016) (abbreviated as CAC from hereon) whose major oxides content respect norm EN 14647 (Calcium aluminate cement, 2007). The Class C and Class F fly ash, OPC, and CAC bulk oxide composition, as determined using X-ray fluorescence (XRF), (Astm, 2004) is detailed in Table 1. The crystalline phases and the quantity of the amorphous phase present were quantified using Quantitative X-Ray Diffraction (QXRD) and Rietveld refinement (Bergmann et al., 1998; Rietveld, 1969). Zincite (ZnO, purity 99.999%) was used as an internal standard at a mass loading of 10 mass %. The Rietveld refinement was conducted using Profex (Doebelin and Kleeberg, 2015). The quantities and types of crystalline phases present in the precursor materials are detailed in Table 2. The Class C fly ash, Class F fly ash, and CAC amorphous content average composition, detailed in Table 1, was calculated by subtracting the crystalline content contribution from the XRF bulk composition. Note that, for CAC, no grossite ($CaAl_2O_7$) was detected, yet this phase can be expected in calcium aluminate cement alongside the other calcium aluminate phases observed and quantified here.(Mangabhai, 2019) As a result, the CAC studied here displays a high amorphous content.

Simulated brines were prepared by dissolving NaCl (99%) or $CaCl_2\cdot 6H_2O$ (99%) in deionized water (DIW) at room temperature under agitation to obtain Cl^- concentration ($[Cl^-]$) of 0.5, 1, and 2 mol/L. Cementitious formulations were prepared by combining 55 mass % of fly ash, 10 mass % of additive and 35 mass % of the brine (i.e., a liquid to solid ratio of 0.54). The formulations were mixed for 45 s at 270 rpm and 1 min at 480 rpm at room temperature using a high-shear immersion mixer. The pastes were poured in hermetic glass bottles and placed into a TamAir isothermal calorimeter at 50 °C for analysis of the resulting heat release. Heat flow and cumulative heat release were measured over 10 days of hydration to assess the rate and the extent of fly ash hydration. The cumulative heat release of the additives (CH, CH-NA, CAC, and OPC) were measured separately in DIW and brines in a system where the fly ash was replaced by quartz (i.e., an inert silicate). The cumulative heat release measured from the additive reaction was subtracted from the value measured in the mixed fly ash/additive systems (Figure S1) to determine the heat release attributed to fly ash reactivity. In general, the heat release showed minimal change ($d\dot{Q}/dt < 0.1$ mW/g/s) after 10 days. The ampoules were retrieved from the calorimeter, and the solid samples were crushed and immediately immersed in isopropanol (IPA) for a week to cease further reaction (Oey et al., 2016). The samples were then dried under vacuum for an additional week, following which they were crushed, milled using an agate pestle and mortar and then sieved through a 300 μm sieve prior to additional characterization.

2.2. Cementitious material characterization

2.2.1. Thermogravimetric analysis

Thermogravimetric analysis (TGA) was performed using a Perkin Elmer STA 8000 under a flow of nitrogen in an aluminum oxide crucible. A heating ramp of 10 °C min^{-1} was used between 35 and 950 °C, after 5 min equilibration at 35 °C. The mass loss (TG) and the derivative mass loss (DTG) were both used to semi-quantify Cl-AFm hydrated phases between ≈250-to-430 °C (Lothenbach et al., 2016; Shi et al., 2017).

2.2.2. X-Ray diffraction

XRD analysis was performed using a PANalytical X'Pertpro diffractometer (θ-θ configuration, CuKα radiation, λ = 1.54 Å) on powder samples spiked with ~10 mass % of ZnO (99.99%). The scans were acquired between 5° and 70° with a step-size of 0.02° using a scientific X'Celerator 2 detector. In general, powdered samples were placed in the sample holder and their surfaces gently textured to minimize the potential for preferred orientation related errors. Rietveld refinement of the samples was performed using the Profex graphical user interface and the BGMN program (Bergmann et al., 1998; Doebelin and Kleeberg, 2015; Rietveld, 1969). The following hydrated phases were identified: ettringite (ICSD #16045), monosulfoaluminate (ICSD #100138), a magnesium-aluminum hydrotalcite-like phase (referred to as

Table 1
The bulk composition and the amorphous content composition (mass %) of the Class C fly ash, Class F fly ash, OPC, and CAC, as determined by XRF (ASTM D4326-04, 2004) and XRD.

	Class C		Class F		OPC		CAC	
	Bulk	Amorphous	Bulk	Amorphous	Bulk	Amorphous	Bulk	Amorphous
CaO	28.0	22.1	4.0	2.6	63.4	–	42.3	14.4
MgO	7.2	3.5	0.9	0.9	1.1	–	0.6	0.4
Al_2O_3	18.5	16.1	20.7	17.9	4.7	–	36.9	13.4
SiO_2	32.0	26.2	52.0	45.9	20.3	–	4.4	2.2
SO_3	3.0	1.9	0.8	0.5	3.0	–	0.1	0.1
Fe_2O_3	5.3	5.2	14.6	10.7	3.7	–	15.5	11.1
Na_2O	1.8	1.8	1.4	1.3	0.1	–	0.1	0.1
K_2O	0.4	0.4	2.4	2.3	0.7	–	0.1	0.2
Others	3.8	3.2	3.2	1.2	3.0	–	0.0	1.6
Total	100.0	80.4	100.0	83.3	100.0	–	100.0	43.5

Table 2
The mineralogical composition (mass %) of the Class C fly ash, Class F fly ash, OPC, and CAC as determined using QXRD.

	Class C	Class F	OPC	CAC
Quartz – SiO_2	5.0	6.0	<1	–
Periclase – MgO	3.3	–	–	–
Free lime – CaO	1.4	0.4	–	–
Merwinite – $Ca_3Mg[SiO_4]_2$	1.7	–	–	–
Magnetite – Fe_3O_4	<1.0	2.1	–	<1.0
Maghemite – γ-Fe_2O_3	–	0.9	–	2.0
Hematite – α-Fe_2O_3	–	0.9	–	–
Portlandite – $Ca(OH)_2$	<0.4 (TGA)	<0.7 (TGA)	–	–
Ye'elimite – $Ca_4Al_6O_{12}SO_4$	0.5	–	–	–
Mullite – $3Al_2O_32{\cdot}SiO_2$	<1.0	5.2	–	–
Anhydrite – $CaSO_4$	1.7	0.6	–	–
Tricalcium aluminate – $Ca_3Al_2O_6$	3.3	–	5.1	5.0
Tricalcium silicate – Ca_3O_5Si	–	–	73.9	–
Dicalcium silicate – Ca_2SiO_4	–	–	8.0	4.3
Tetracalcium aluminoferrite – $Ca_4Al_2Fe_2O_{10}$	–	–	13.8	10.0
Gypsum – $CaSO_4{\cdot}2H_2O$	–	–	4.4	–
Monocalcium aluminate – $CaAl_2O_4$	–	–	–	30.6
Gibbsite – $Al(OH)_3$	–	–	–	1.9
Mayenite – $Ca_{12}Al_{14}O_{33}$	–	–	–	2.2
Sum of crystalline phases	19.6	16.7	100	56.5
Amorphous phases	80.4	83.3	0.0	43.5

hydrotalcite from hereon, PDF #00–014-0525), katoite (ICSD #34227), Kuzel's salt (PDF #00-019-0203), Friedel's salt (ICSD #62363), and strätlingite (PDF #29-0285).

2.2.3. Infrared spectroscopy

Solid-state attenuated total reflection Fourier-transform infrared spectroscopy (ATR-FTIR) was performed using a Spectrum Two FT-IR Spectrometer (Perkin Elmer). The powdered samples were pressed using around 90 N of force onto a diamond/ZnSe composite crystal to ensure good contact and generate total internal reflection. The spectra reported herein were obtained by averaging 4 scans over the wavenumber range of 4000-to-400 cm^{-1} at a resolution of 1 cm^{-1}.

2.3. Thermodynamic modeling

Thermodynamic modeling was conducted using GEM-Selektor v.3.6 (GEMS) (Kulik et al., 2012; Wagner et al., 2012) which incorporates the slop98.dat and Cemdata18 thermodynamic databases (Hummel et al., 2002; Johnson et al., 1992; Lothenbach et al., 2019, 2008; Thoenen et al., 2014). To represent the non-ideality of the solutions, the activity coefficients were calculated using the Truesdell-Jones extension to the Debye-Hückel equation (Helgeson et al., 1981, p. 198):

$$\log_{10}\gamma_i = \frac{-A_\gamma z_i^2\sqrt{I}}{1+\dot{a}B_\gamma\sqrt{I}} + b_\gamma I + \log_{10}\frac{X_{jw}}{X_w} \quad (1)$$

where, γ_i is the activity coefficient and z_i the charge of the i^{th} aqueous species, A_γ and B_γ are temperature and pressure dependent coefficients, X_{jw} is the molar quantity of water, X_w is the total molar amount of the aqueous phase, and I is the molal ionic strength. A common ion size parameter (a = 3.72 Å) and a short-range interaction parameter (b_γ = 0.64 kg mol^{-1}) were used, treating NaCl as the background electrolyte (Helgeson et al., 1981; Vollpracht et al., 2016). All concentrations (up to 2 mol/L of Cl^-) were considered to conform to the limits of applicability using Eq. (1). Of course, as water is consumed over the course of reaction, the concentration sometime exceeds the 2 mol/L limit. As such, some uncertainty is expected in the quantitative (although not qualitative) analysis (Kulik et al., 2012; Langmuir, 1998). The system modeled (55 g of FA, 10 g of portlandite, and 35 g of brine) is similar to that studied experimentally, and follows a model previously developed for similar Class C and Class F fly ashes (Collin et al., 2021). Briefly, the additives are considered to be completely hydrated, except for CAC in presence of Class F: in this system, only the CAC crystalline content reaction is considered to accurately reproduce experimental results. Note that this is consistent with the literature observation that CAC typically displays sequential reactivity for both its crystalline and amorphous content, with calcium aluminate reaction kinetics being faster than other phases (e.g., grossite).(Sorrentino et al., 1995; Klaus et al., 2013; Goergens et al., 2023) The fly ashes are considered to show fractional reactivity based on: (a) the lack of reaction of the insoluble crystalline phases (e.g., quartz), (b) incomplete reaction of some partially soluble crystalline phases, (c) complete consumption of the highly-reactive crystalline phases (e.g., $CaSO_4$), and (d) the congruent dissolution of the amorphous phase given its average composition (Table 1) (Collin et al., 2021). The degree of fly ash reaction after 10 days of hydration at 50 °C is determined by analyzing when the ratio of well-characterized crystalline phase masses, e.g., portlandite (CH: $Ca(OH)_2$), is equal to unity; i.e., when the modeled quantity of a given phase is equivalent to its content established by experimental (TGA and/or XRD assessments, e.g., when $CH_m/CH_e \approx 1$, where the subscripts 'm' and 'e' indicate modeled and experimental assessments).

2.4. Machine learning modeling

An artificial-neural-network-based machine learning model was developed to predict the fly ash degree of reaction (FA DR) from the initial setup composition. Based on the experimental results collected herein and from a previous study (Collin et al., 2021), a dataset of 70 samples was curated to assess the FA DR under various combinations of fly ash type, additive type, and brine composition and concentration. For each sample, the inputs comprise a total of nine features corresponding to (1) the type of fly ash (i.e., Class C or Class F), (2) the type of additives

(i.e., CH/CH-NA/OPC/CAC), and (3) the ions molar concentrations (i.e., $Na^+/Ca^{2+}/Cl^-$). To limit the dimensionality of the model (so as to avoid the "curse of dimensionality") (Liu et al., 2019; Ouyang et al., 2020), the fly ash and additive inputs were set as categorical features as either "applied" or "not applied" using the one-hot encoding approach (Pargent, 2019), while the brine concentrations were provided based on the actual experimental values. The neural network and all related analyses were built and implemented within PyTorch (an open-source machine learning platform), with Adam as the optimizer, Rectified Linear Unit (ReLU) as the activation function, and L2 norm as the cost function (Paszke et al., 2019). To avoid the overfitting issue typically associated with complex machine learning models (which usually results in a false positive estimation of the model accuracy and poor generalizability for predicting new samples) (Ouyang et al., 2021), the artificial neural networks were all designed with a relatively simple structure comprising six artificial neurons (i.e., one-tenth of the training samples) in a single hidden layer by following commonly used guidelines (Heaton, 2008). Following common practices in machine learning, 52 samples (i.e., ~75% of the dataset as "training set") were allocated for training the neural network, while the remaining 18 samples (i.e., ~25% of the dataset as "test set") were kept hidden from the model during training. Here, the test set was used to quantify the ability of the model to generalize, that is, to accurately predict reactivity in unknown conditions (that were not used to train the model). Considering the limited size of the dataset, the train-test split was conducted using stratification sampling to ensure that the split subsets follow the same distribution of the original dataset—so that the train and test sets are statistically aligned (Jablonka et al., 2020; Ouyang et al., 2021; Song et al., 2021a). To ensure that the obtained results are not biased by the choice of the test set, ten independent neural networks models were trained based on ten different stratified train-test splits. The results reported herein are based on the average of those ten neural networks. The settings of the artificial neural networks (i.e., hyperparameters) (Demir-Kavuk et al., 2011) were optimized by cross-validation based on a grid search within a given reasonable range for each hyperparameter (i.e., 10^{-1}-to-10^{-3} for learning rate and 10^{-2}-to-10^{-5} for weight decay; with ten intervals on each magnitude). Based on the average validation set accuracy, the optimal learning rate and weight decay were chosen as 10^{-2} and 2×10^{-2}.

3. Results and discussion

3.1. Effect of additive type on phase assemblage and fly ash reactivity in the absence of brine

The hydrated phase assemblage formed after 10 days of hydration at 50 °C of a system containing 55 mass % of fly ash (Class C or Class F), 10 mass % of additive (two types of cement, lime with and without $NaAlO_2$), and 35 mass % of DIW was assessed using XRD (Fig. 1).

Using portlandite only as an additive (i.e., CH systems) results in the formation of amorphous C-S-H (peak around 950 cm^{-1} in the IR spectrum, Fig. 1b and d) as a result of the pozzolanic reaction between portlandite and the silicate content of the fly ashes for both Class C and Class F fly ash. Monosulfoaluminate (main peak at 9.93° 2θ in the XRD pattern), katoite (32.61° 2θ), and hydrotalcite (11.63° 2θ) are also observed within the Class C fly ash system (Fig. 1a), due to the joint hydrolysis of Al and Mg during the pozzolanic reaction. Ettringite (9.08° 2θ) and monosulfoaluminate only are observed within the Class F fly ash system due to Class C fly ash lower reactivity (Fig. 1c).

Using portlandite + $NaAlO_2$ as an additive (i.e., CH-NA system) still induce the formation of C-S-H when combined with the Class F fly ash, but only ettringite is observed to form alongside the C-S-H. This suggests that the Class F fly ash reactivity is limited when combined with CH-NA. Similarly, a strong decrease in the amount of crystalline phase formation is observed with the Class C fly ash, where the only major hydrate phases detected are the C-S-H phases (Fig. 1b), as well as traces of katoite and potentially strätlingite. $NaAlO_2$ dissolution (to form NaOH and $Al(OH)_3$) was observed to consume a significant fraction of the water initially available and produced a strongly alkaline solution where the formation of some crystalline phases (such as monosulfate) may be suppressed (Collin et al., 2021).

Using OPC as an additive (i.e. OPC system) results in the formation of C-S-H and ettringite with the Class F fly ash (Fig. 1c), suggesting again a lower reactivity of the fly ash compared to that observed with portlandite. With the Class C fly ash, the phase assemblage is similar to that observed in the CH system. This suggests that both fly ash pozzolanic reaction is not strongly affected by the delayed portlandite formation from OPC hydration.

Finally, using CAC as an additive results in the formation of C-S-H with Class C fly ash (Fig. 1b), as well as strätlingite (7.00° 2θ) which forms preferentially in this system instead of katoite (Fig. 1a). With the Class F fly ash, strätlingite is also observed to form (Fig. 1c) and appears to suppress amorphous C-S-H formation (Fig. 1d). Strätlingite and katoite or C-S-H can typically coexist in cementitious systems, although strätlingite formation is favored in high Al-containing systems (Okoronkwo and Glasser, 2016). Here, the formation of strätlingite consumes all the available Al and Si in the systems, which suppresses the formation of other phases.

The experimental phase assemblages were all successfully reproduced using thermodynamic, allowing for the determination of the fly ash degree of reaction (FA DR) after 10 days of reaction at 50 °C. A strong difference in reactivity is observed between the Ca-rich Class C fly ash (DR value above 10 mass % regardless of the additive used, Fig. 2a) and the Ca-poor Class F fly ash (DR value below 6 mass % regardless of the additive used, Fig. 2b), which is consistent with previous observations (Oey et al., 2017b; Song et al., 2021b). Such differences in

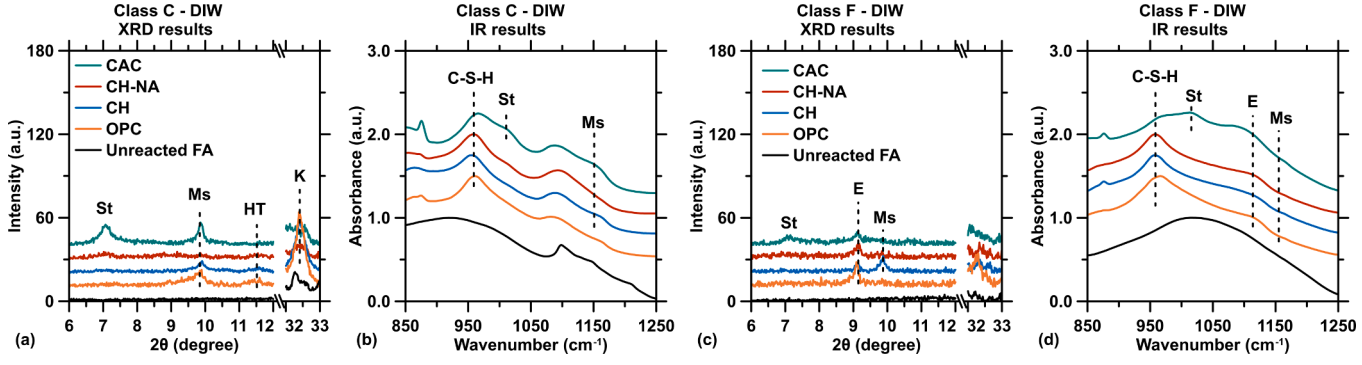

Fig. 1. The crystalline and amorphous hydrated phases formed, as determined using XRD (with background subtraction) and IR spectroscopy. **(a)** XRD diffractograms and **(b)** IR spectra obtained for the hydrated Class C fly ash with the additives in DIW. **(c)** XRD diffractograms and **(d)** IR spectra obtained for the Class F fly ash with the additives in DIW. E = ettringite, Ms = monosulfoaluminate, St = strätlingite, HT = hydrotalcite, K = Katoite.

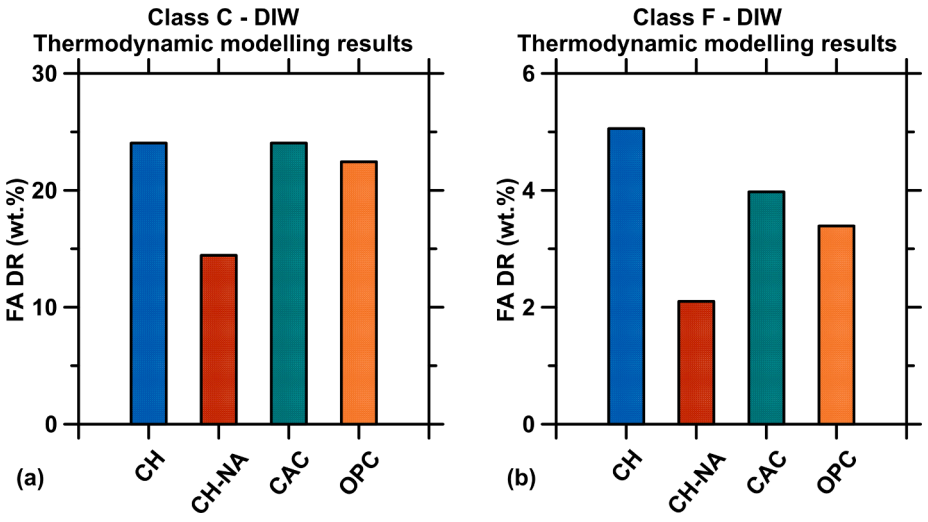

Fig. 2. The fly ashes degree of reaction (FA DR) as determined using thermodynamic modeling for **(a)** the Class C fly ash with the additives in DIW, and **(b)** the Class F fly ash with the additives in DIW.

reactivity are related to the amorphous content network topology: a Ca-rich fly ash network is usually less constrained (connected) than that of a Ca-poor Class F fly ash as per the topological constraint theory (TCT) (Bauchy, 2019; Mauro, n.d.; Oey et al., 2017b; Song et al., 2021b). Silicates with less constrained structure commonly show higher silicate dissolution rate in aqueous medium (Oey et al., 2017a; Pignatelli et al., 2016), and are also expected to be more reactive in cementitious systems (Oey et al., 2017b). For both Class C and Class F fly ashes, the highest fly ash extent of reaction is observed when combined with portlandite (i.e., CH system). The Class C fly ash reactivity in OPC and CAC systems is similar to that observed in the CH system. In contrast, the Class F fly ash reactivity in OPC and CAC is notably lower than that observed in the CH system. This suggests that the lowly reactive Class F fly ash is more sensitive to additive composition changes than the highly reactive Class C fly ash, as its reactivity relies more strongly on the pozzolanic and hydration reaction. Finally, for both Class C and Cass F fly ash, CH-NA induces a strong decrease in fly ash reactivity, as it was observed to limit the formation of several crystalline phases in both Class C and Class F system.

3.2. *Effect of brine concentration on the phase assemblage and fly ash reactivity*

The hydrated phase assemblage formed after 10 days of hydration at 50 °C of the fly ash/additive system is assessed when combined with brine (NaCl or $CaCl_2$ with $0.5 \leq [Cl^-] \leq 2$ M). Results obtained for $[Cl^-]$

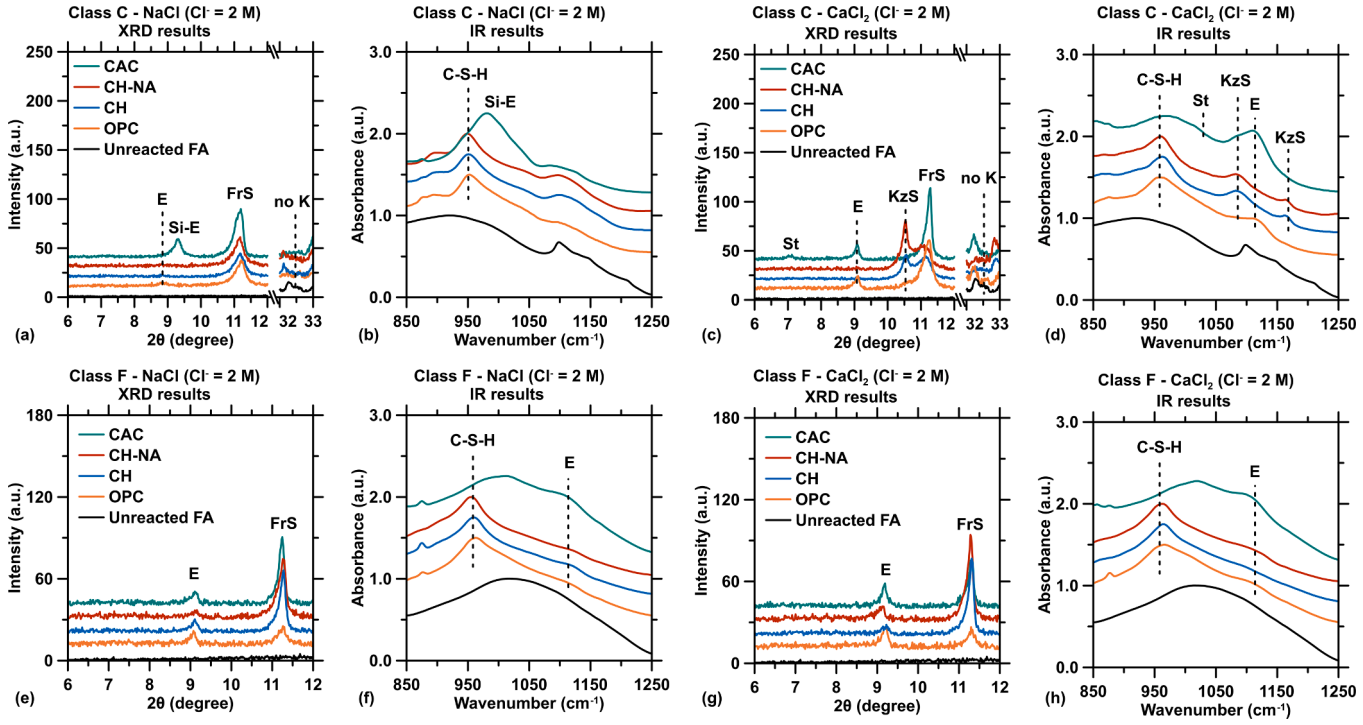

Fig. 3. The crystalline and amorphous hydrated phases observed experimentally with brines ($[Cl^-] = 2$ M), for the Class F fly ash in **(a)** & **(b)** NaCl and **(c)** & **(d)** $CaCl_2$ brine; and for the Class C fly ash in **(e)** & **(f)** NaCl and **(g)** & **(h)** $CaCl_2$ brine. E = ettringite, Si-E = Si-containing ettringite-like phase, St = strätlingite, K = katoite, FrS = Friedel's salt, and KzS = Kuzel's salt.

= 2 M are displayed in Fig. 3 as an illustration. For the Class C fly ash, a broad range of hydrated phases is observed as a function of the type of brine and the type of additive. In the presence of NaCl, the main hydrate phases forming are C-S-H and Friedel's salt (11.20° 2θ) in the OPC, CH, and CH-NA systems (Fig. 3a). In the CAC system, the shift of the peak from 9.08° 2θ to 9.26° 2θ in the XRD pattern, and the position of the peak at ~980 cm^{-1} in the IR spectrum both suggest that the AFt phase forming at high NaCl content may be a Si-containing ettringite-like phase with a composition in between that of ettringite ($Ca_6Al_2(OH)_{12}(SO_4)_3{\cdot}24H_2O$) (Matschei et al., 2007) and kottenheimite ($Ca_3Si(OH)_6(SO_4)_2{\cdot}12H_2O$) (Chukanov et al., 2012). In the presence of $CaCl_2$, mixed formation of C-S-H, strätlingite, ettringite, Kuzel's (9.89° 2θ) and/or Friedel's salt is observed in varying quantity depending on the additives considered (Fig. 3b). For the Class F fly ash, similar crystalline phases – ettringite and Friedel's salt – are observed regardless of the type of salt or the type of additive (Fig. 3c and d). The main difference observed as a function of the additive type is the absence of C-S-H in CAC system, as was the case in DIW. These results highlight that, in the presence of Cl^- ions, Cl-AFm are the predominant phases forming regardless of the type of additive used. Cl-AFm easily destabilize other hydrates previously observed in DIW, such as strätlingite, katoite, or monosulfoaluminate (Birnin-Yauri and Glasser, 1998; Glasser et al., 1999). while the amorphous C-S-H remains unchanged. The differences observed between NaCl and $CaCl_2$ were shown in previous study to be related to differences in the pore solution pH: Na^+ lower incorporation in hydrated phases – as opposed to Cl^- and Ca^{2+} – induces the formation of OH^- via the dissociation of water to ensure charge neutrality of the solution, resulting in a strong increase in the pore solution pH (Collin et al., 2021). This, in turn, affects the phase assemblage.

Increasing Cl-AFm formation is observed with increasing Cl^- concentration regardless of the type of fly ash, the type of additive, and the type of salt (Fig. 4). For the Class C fly ash, different trends of Cl-AFm formation are observed depending on the type of salt in the brine. With NaCl, higher content of Cl-AFm content is observed with OPC up to $[Cl^-]$ = 1 M, but above that value higher formation is observed with CAC (Fig. 4a). With $CaCl_2$, higher Cl-AFm contents are observed with CH and CH-NA at $[Cl^-]$ = 2 M, while OPC display higher Cl-AFm formation at lower concentration (Fig. 4b). However, both Kuzel's and Friedel's salts form in CH and CH-NA systems, while only Friedel's salt forms in OPC system. This suggests that the OPC system might be able to encapsulate more Cl^- as Friedel's salt retains twice as much Cl^- as Kuzel's salt. For the Class F fly ash, the highest Cl-AFm formation regardless of the brine type is attained in the CH-NA system (Fig. 4c and d), although the difference with the CH system is minimal.

The fly ash reactivity as a function of the brine type was determined experimentally (cumulative heat release) and using thermodynamic modeling (fly ash DR). All brine systems were successfully modeled, except for five setups showing limitation of the congruent dissolution model used for the Class C fly ash. The five missing setups FA DR were calculated based on the linear correlation found between the cumulative heat release and the successfully modeled fly ash DRs (Figure S2). All the results are displayed in Fig. 5. The Class C fly ash reactivity decreases regardless of the additive type in brines with $[Cl^-] < 2$ M compared to DIW. This is due to the preferential formation of Cl-AFm that cannot counteract the inhibition of other hydrates formation: in DIW, the highly reactive Class C fly ash reaction led to the formation of Ca- and Al-containing hydrated phases such as monosulfoaluminate, katoite and/or strätlingite. Monosulfoaluminate and katoite are shown to be unstable in Cl-containing brines due to Cl^- capacity to incorporate in AFm phases, yet the amount of Cl-AFm forming at Cl^- concentration < 2 M ($CaCl_2$ and NaCl both) is lower than the amount of monosulfoaluminate and katoite formed in DIW. For $[Cl^-] > 2$ M, several systems show an increase in fly ash reactivity. The Class C + CAC + 2 M NaCl system (Fig. 5a) shows the significant formation of a Si-containing ettringite-like phase that induces a resurgence of fly ash reactivity. This phase formation is constrained to high pH (~13) and high Si, Ca, and Al-containing systems. In the $CaCl_2$ brine systems (Fig. 5b), an increase in reactivity is observed in the CH and CH-NA systems, but not in the OPC and CAC systems despite both systems showing high Friedel's salt formation (Fig. 3b). This highlights the fact that, in the OPC and CAC systems, Cl-AFm formation comes primarily from the additive hydration, as opposed to the CH and CH-NA systems where the Cl-AFm formation requires strong fly ash reaction.

Class F fly ash reactivity (Fig. 5c and d) increases with increasing Cl^- concentration only in the systems with high Ca and low Al content additive (i.e., the CH or CH-NA systems). Cl-AFm formation has been observed to be a driver of the Class F fly ash reactivity in brines (Collin et al., 2021), as it requires Al extraction from the fly ash amorphous content. In contrast, the Class F fly ash reactivity decreases with increasing Cl^- concentration in a system with high Ca and Al content (i.e., the CAC system). Cl-AFm formation appears to be detrimental to strätlingite formation, which was shown to strongly influence the fly ash reactivity in DIW, as it required additional Al and Si extraction from the fly ash amorphous content. Cl-AFm phases, in contrast, can form with the Ca and Al content directly provided by the additive. They do not require high levels of dissolution from the amorphous content to form, resulting in a decrease of fly ash reactivity compared to that observed in DIW. The OPC system, with low Cl-AFm formation and high C-S-H formation, is less impacted than the other systems by brine concentration. In this system, the Class F fly ash hydration results in the further formation of C-S-H, which is unaffected by Cl^- concentration.

3.3. Predicting the fly ash degree of reaction

The broad range of FA DR observed in the previous section raises an issue regarding the capacity to predict an S&S mix performance.

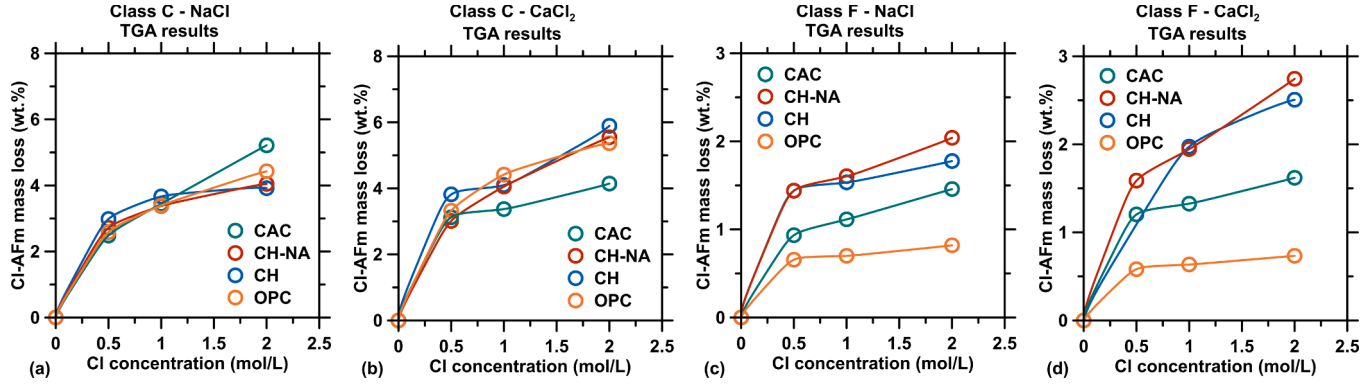

Fig. 4. The Cl-AFm (Kuzel's and Friedel's salts) mass loss measured between ~ 270 and 400 °C using TGA for the Class C fly ash in **(a)** NaCl and **(b)** $CaCl_2$ brine, and the Class F fly ash in **(c)** NaCl and **(d)** $CaCl_2$ brine. Note that one aberrant datapoint (Class F fly ash + CH + 0.5 M $CaCl_2$) is excluded from the dataset.

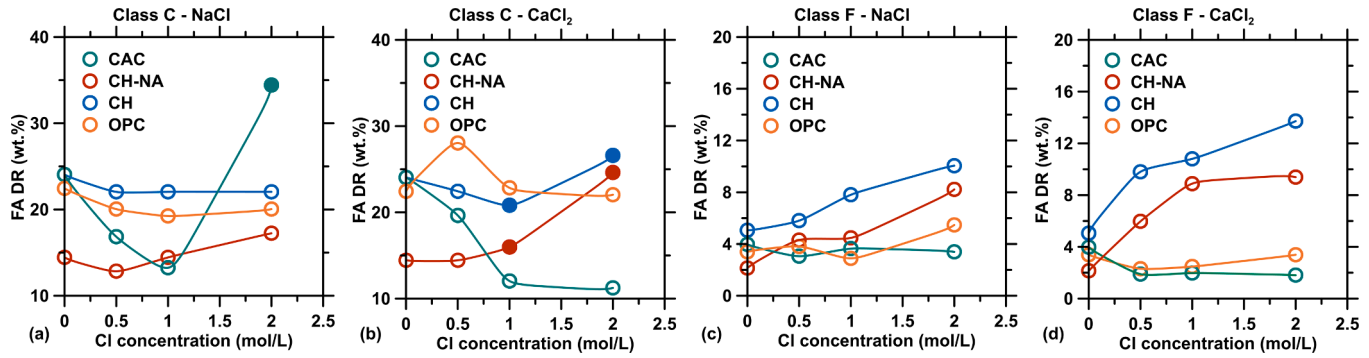

Fig. 5. The fly ash degree of reaction (FA DR) as determined from thermodynamic modeling for the Class C fly ash with the additives in **(a)** NaCl and **(b)** $CaCl_2$ brine, and the Class F fly ash with the additives in **(c)** NaCl and **(d)** $CaCl_2$ brine. The five full symbols indicate the FA DR that were estimated from the experimental heat release value (Figure S2) instead of directly modeled.

Thermodynamic modeling has been proven to be a fast and reliable tool to accurately predict phase assemblage at near-equilibrium. It can therefore be used to assess multiple S&S systems' performance and help reduce the number of experiments needed to develop the ideal fly ash + additive + brine solution as a function of the materials available and the brine produced. However, thermodynamic modeling of fly-ash-containing systems, as used here or in previous studies (Collin et al., 2021; Glosser et al., 2020). relies on using empirical data to perfectly assess the phase assemblage at equilibrium. Gathering experimental data for all systems that need to be studied is not feasible in terms of time and cost, yet choosing the DR can be fairly arbitrary, given the strong dependence of DR on the initial system composition as previously demonstrated. As a result, the modeled phase assemblage obtained using an arbitrary DR may significantly deviate from reality. This highlights the need to develop more robust methods to determine the fly ash degree of reaction of a specific system. In that regard, machine learning models have been proven to be powerful in their capacity to predict physical or chemical behaviors, even based on sparse datasets (Oey et al., 2020; Ouyang et al., 2020; Song et al., 2021a). The total number of datapoints – 70 datapoints – collected here (54 datapoints) and from a previous work (Collin et al., 2021) that studied a similar type of dataset (i.e., same fly ashes mixed with portlandite and NaCl or $CaCl_2$ brines, 16 datapoints) was deemed large enough to be implemented in an artificial neural network-based machine learning model to predict the DR as a function of the initial setup composition (i.e., the type of fly ash, additive, and brine). The assessment of the model prediction demonstrates a satisfactory accuracy (Fig. 6a), as supported by the sufficiently high coefficient of determination ($R^2 = 0.96$), the low root mean square error (RMSE = 1.8 wt%), and the low mean absolute percentage error (MAPE = 10%) of the test set samples that are never exposed to the model during its training. This confirms the model's capacity to accurately predict the fly ash DR of systems that falls within the broad range of compositions studied herein. With this, a realistic DR can be considered to thermodynamically model the hydrated system at near-equilibrium and to select the best performing S&S mix.

In addition to offering predictions of fly ash DR that can be used to pinpoint optimal S&S mixtures, the machine learning model makes it possible to robustly isolate and quantify the influence of each variable on fly ash reactivity in accordance to experimental observations (refer to supplementary information and Figure S3 for the rank of impact on DR from the different features). Herein, the model offers realistic extrapolations, that is, can predict the DR beyond the setup compositions involved in the experiments, for example at higher brine concentrations. The relevant predictions are illustrated based on the feature effect analysis (refer to supplementary information for more information on the analytical technique), an example of which is presented in Fig. 6b and c. Here, the sole effect of Cl^- concentration is studied, so as to further isolate the effect of Cl^- concentration from that of the counter-ions. Isolating the effect of Cl^- is not easily done from experimental observations, the model thus offers further knowledge regarding the brine composition and concentration effect on fly ash reactivity. Continuous predictions are made as a function of Cl^- concentration under the various combinations of fly ashes and additives. The predicted DR values are shown to encompass all the experimental values within error. This suggests that the predicted value outside of the dataset range, though they are displaying increased uncertainties (see supplementary information for details), should also be able to capture the various effects of each feature and predict an appropriate FA DR for further thermodynamic modeling of the system.

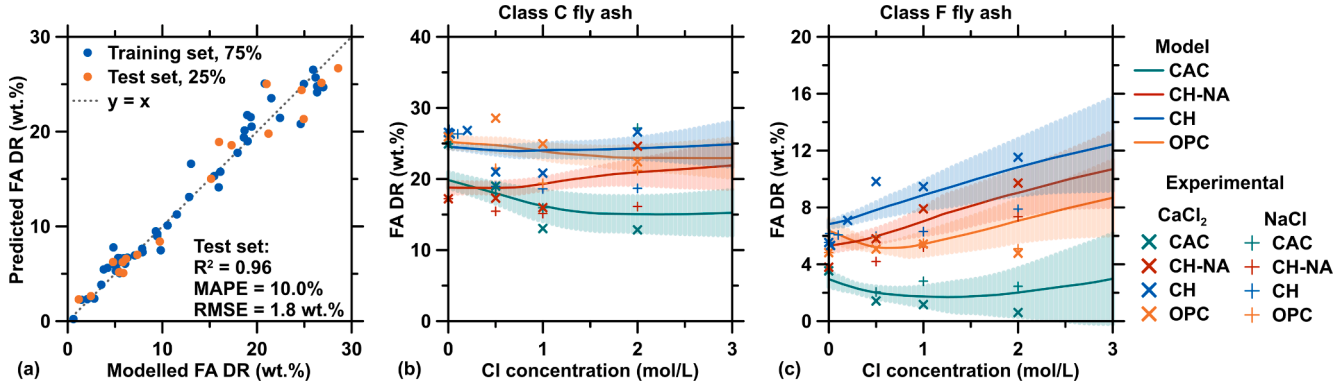

Fig. 6. The neural-network-based machine learning analysis. **(a)** The comparison between predicted vs. "true" fly ash degree of reaction (FA DR) obtained from thermodynamic modeling. The feature effect analysis focusing on Cl^- concentration effect for **(b)** the Class C and **(c)** the Class F fly ash; the results are obtained from averaging ten individually trained models, with the mean and standard deviation displayed as the solid line and shadow, respectively.

3.4. Additional considerations and final recommendations

All the results compiled here show that, as expected (Song et al., 2021b), the Class C fly ash will always be more reactive than the Class F fly ash regardless of the type of brine or the additive with which it is combined. Higher reactivity usually implicates higher phase formation, and as a result higher brine consumption and lower porosity, all of which are beneficial for S&S systems (Okoronkwo et al., 2018). Indeed, all these parameters ensure good performances for encapsulation/immobilization of pollutants that can either be incorporated or sorbed in hydrated phases (e.g., alkali ions and halide anions), or can precipitate as insoluble species whose migration is constrained by the low porosity (e.g., heavy metals). However, when studying various additive effects, the system performance is assessed based on the degree of Cl-AFm formation (i.e., the amount of Cl^- effectively retained within the solid). Indeed, while portlandite is typically observed to be the best additive to promote fly ash reactivity, it does not necessarily induce the highest Cl-AFm formation compared to other additives. In general, the Class C fly ash combined with high NaCl concentration brines (above 1 M of Cl^-) showed the best performances when combined with CAC. At lower concentration (below 1 M of Cl^-), OPC provided the best performance. For $CaCl_2$ brines, combining a Class C fly ash with OPC also offers the best performance regardless of the brine concentration. When using a class F fly ash, a mix of portlandite and $NaAlO_2$ as an additive is shown to slightly decrease the fly ash reactivity compared to portlandite only yet allows for a low increase in hydrated phase formation. The choice of using $NaAlO_2$ or not is therefore a cost-effective one, as portlandite provides near-similar performances regardless of the brine type (NaCl or $CaCl_2$) and concentration. Finally, at higher concentrations than the one studied here, it is recommended to evaluate the various setup using thermodynamic modeling and considering the predicted FA DR range depicted in Fig. 6c and d.

4. Summary and conclusion

This study demonstrates the combined effect of the fly ash type and the additive composition on (1) the fly ash reactivity, and (2) the final solid capacity to successfully encapsulate the chloride-contaminant from two types of brine (NaCl and $CaCl_2$). Increasing Ca content (either from the fly ash or the brine) induces an increase in the fly ash reactivity – Class C and Class F both. Utilizing OPC, CAC, or mixed Portlandite-$NaAlO_2$ as additives results in a decrease of both Class C and Class F fly ashes reactivity in Cl-containing systems. In contrast, portlandite combined with high Cl^- concentration (i.e., >1 M) generally induces an increase in fly ash reactivity. An important observation is that higher fly ash reactivity is not necessarily correlated with the highest preferred hydrate phase formation (i.e., Cl-AFm). Some additives (e.g., OPC) may hinder the fly ash reactivity, yet produce hydrate phases independent of fly ash hydration. As a result, choosing the appropriate fly ash + additive + brine mix is not trivial. While choosing a Class C over a Class F fly ash is always the better option, the choice of the additive type is extremely sensitive to the brine composition and concentration. The experimental work done here proposes some recommendation within the range of composition studied experimentally, and the machine learning model can be applied in the future to select appropriate mixture proportions outside of the range studied (e.g., higher brine concentration) by predicting the fly ash degree of reaction that can then be used to refine thermodynamic modeling predictions of S&S performance.

Declaration of Competing Interest

The authors declare that they have no known competing financial interests or personal relationships that could have appeared to influence the work reported in this paper.

Data availability

Data will be made available on request.

Acknowledgment

The authors acknowledge financial support for this research provided by the Electric Power Research Institute (EPRI), the U.S. Department of Transportation through the Federal Highway Administration (grant no. 693JJ31950021), and the U.S. National Science Foundation (DMREF: 1922167). The contents of this paper reflect the views and opinions of the authors, who are responsible for the accuracy of data presented herein. This research was conducted in the Laboratory for the Chemistry of Construction Materials (LC^2) and the Molecular Instrumentation Center (MIC) at the University of California, Los Angeles (UCLA). As such, the authors acknowledge the support that has made these laboratories and their operations possible.

Appendix A. Supplementary data

Supplementary data to this article can be found online at https://doi.org/10.1016/j.wasman.2023.08.002.

References

ASTM D4326-04, 2004. Standard test method for major and minor elements in coal and coke ash by X-ray fluorescence. ASTM International, West Conshohocken, PA.
ASTM C618, 2019. Specification for Coal Fly Ash and Raw or Calcined Natural Pozzolan for Use in Concrete. ASTM International, West Conshohocken, PA. https://doi.org/10.1520/C0618-17A.
Bauchy, M., 2019. Topological Constraint Theory and Rigidity of Glasses, in: Sattler, K.D. (Ed.), 21st Century Nanoscience – A Handbook. CRC Press, Boca Raton, Florida : CRC Press, [2020], pp. 13-1-13–20. https://doi.org/10.1201/9780367333003-13.
Bergmann, J., Friedel, P., Kleeberg, R., 1998. BGMN - a new fundamental parameters based Rietveld program for laboratory X-ray sources, it's use in quantitative analysis and structure investigations. Commission on Powder Diffraction (IUCr) 20, 5–8.
Birnin-Yauri, U.A., Glasser, F.P., 1998. Friedel's salt, $Ca_2Al(OH)_6(Cl,OH)\cdot 2H_2O$: its solid solutions and their role in chloride binding. Cement and Concrete Research 28, 1713–1723. https://doi.org/10.1016/S0008-8846(98)00162-8.
Borch, T., Dionysiou, D., Katz, L., Xu, P., Breckenridge, R., Ellison, K., Fox, J., Macknick, J., Sedlak, D., Stokes-Draut, J., 2021. National Alliance for Water Innovation (NAWI) Technology Roadmap: Agriculture Sector.
Calcium aluminate cement.: Composition, specifications and conformity criteria, 2007. BSI, London.
Cath, T., Chellam, S., Katz, L., Breckenridge, R., Cooper, C.A., Ellison, K., Macknick, J., McKay, C., Miller, K., Monnell, J., Rao, N., Rosenblum, J., Sedlak, D., Stokes-Draut, J., 2021a.
Cath, T., Chellam, S., Katz, L., Kim, J., Breckenridge, R., Macknick, J., Meese, A., Monnell, J., Rogers, T., Sedlak, D., Seetharaman, S., Stokes-Draut, J., 2021b. National Alliance for Water Innovation (NAWI) Technology Roadmap: Industrial Sector.
Childress, A., Giammar, D., Jiang, S., Macknick, J., Plata, S., Sedlak, D., Stokes-Draut, J., Breckenridge, R., Howell, A., 2021. National Alliance for Water Innovation (NAWI) Technology Roadmap: Power Sector.
Chukanov, N.V., Britvin, S.N., Van, K.V., Mockel, S., Zadov, A.E., 2012. Kottenheimite, $Ca_3Si(oh)_6(SO_4)_2.12H_2O$, a new member of the ettringite group from the Eifel area, Germany. Canadian Mineralogist 50, 55–63. https://doi.org/10.3749/canmin.50.1.55.
Collin, M., Prentice, D.P., Arnold, R.A., Ellison, K., Simonetti, D.A., Sant, G.N., 2021. Fly Ash–$Ca(OH)_2$ Reactivity in Hypersaline NaCl and $CaCl_2$ Brines. ACS Sustainable Chem. Eng. 9, 8561–8571. https://doi.org/10.1021/acssuschemeng.1c01884.
Collin, M., Prentice, D.P., Arnold, R.A., Ellison, K., Simonetti, D.A., Sant, G.N., 2022. How Brine Composition Affects Fly Ash Reactions: The Influence of (Cat-, An-)ion Type. Adv. Civ. Eng. Matls. 11, 20210155. https://doi.org/10.1520/ACEM20210155.
Damidot, D., Lothenbach, B., Herfort, D., Glasser, F.P., 2011. Thermodynamics and cement science. Cem. Concr. Res. 41, 679–695. https://doi.org/10.1016/j.cemconres.2011.03.018.
Demir-Kavuk, O., Kamada, M., Akutsu, T., Knapp, E.-W., 2011. Prediction using stepwise L1, L2 regularization and feature selection for small data sets with large number of features. BMC Bioinf. 12, 412. https://doi.org/10.1186/1471-2105-12-412.
Doebelin, N., Kleeberg, R., 2015. Profex: a graphical user interface for the Rietveld refinement program BGMN. J. Appl. Crystallogr. 48, 1573–1580. https://doi.org/10.1107/S1600576715014685.
Ellison, K., 2019. Landfill Sequestration of Brine: Research Updates 15.
Fatoba, O.O., Petrik, L.F., Akinyeye, R.O., Gitari, W.M., Iwuoha, E.I., 2013. Laboratory Study on the Mobility of Major Species in Fly Ash-Brine Co-disposal Systems: Up-

flow Percolation Test. Water Air Soil Pollut. 224, 1724. https://doi.org/10.1007/s11270-013-1724-9.
Fatoba, O.O., Petrik, L.F., Akinyeye, R.O., Gitari, W.M., Iwuoha, E.I., 2015. Long-term brine impacted fly ash. Part 1: chemical and mineralogical composition of the ash residues. Int. J. Environ. Sci. Technol. 12, 551–562. https://doi.org/10.1007/s13762-013-0439-1.
Giammar, D., Jiang, S., Xu, P., Breckenridge, R., Edirisooriya, T., Jiang, W., Lin, L., Macknick, J., Rao, N., Sedlak, D., Stokes-Draut, J., Xu, X., 2021. National Alliance for Water Innovation (NAWI) Technology Roadmap: Municipal Sector.
Glasser, F.P., 1997. Fundamental aspects of cement solidification and stabilisation. J. Hazard. Mater. 52, 151–170. https://doi.org/10.1016/S0304-3894(96)01805-5.
Glasser, F.P., Kindness, A., Stronach, S.A., 1999. Stability and solubility relationships in AFm phases Part I. Chloride, sulfate and hydroxide. Cem. Concr. Res. 29, 861–866. https://doi.org/10.1016/S0008-8846(99)00055-1.
Glosser, D., Suraneni, P., Isgor, O.B., Weiss, W.J., 2020. Estimating reaction kinetics of cementitious pastes containing fly ash. Cem. Concr. Compos. 112, 103655 https://doi.org/10.1016/j.cemconcomp.2020.103655.
Goergens, J., Belli, R., Schulbert, C., Goetz-Neunhoeffer, F., 2023. Influence of different CA_2/CA-ratios on hydration degree, AH_3 content and flexural strength investigated for a binder formulation of calcium aluminate cement with calcite. Cem. Concr. Res. 165, 107090 https://doi.org/10.1016/j.cemconres.2023.107090.
Gougar, M.L.D., Scheetz, B.E., Roy, D.M., 1996. Ettringite and C-S-H Portland cement phases for waste ion immobilization: A review. Waste Manag. 16, 295–303. https://doi.org/10.1016/S0956-053X(96)00072-4.
Guide to the selection and use of hydraulic cements, 2016.
Heaton, J., 2008. Introduction to Neural Networks with Java. Heaton Research Inc.
Helgeson, H.C., Kirkham, D.H., Flowers, G.C., 1981. Theoretical prediction of the thermodynamic behavior of aqueous electrolytes by high pressures and temperatures; IV, Calculation of activity coefficients, osmotic coefficients, and apparent molal and standard and relative partial molal properties to 600 degrees C and 5kb. Am. J. Sci. 281, 1249–1516. https://doi.org/10.2475/ajs.281.10.1249.
Hummel, W., Berner, U., Curti, E., Pearson, F.J., Thoenen, T., 2002. Nagra/PSI Chemical Thermodynamic Data Base 01/01. Radiochim. Acta 90. https://doi.org/10.1524/ract.2002.90.9-11_2002.805.
Jablonka, K.M., Ongari, D., Moosavi, S.M., Smit, B., 2020. Big-Data Science in Porous Materials: Materials Genomics and Machine Learning. Chem. Rev. acs.chemrev.0c00004. https://doi.org/10.1021/acs.chemrev.0c00004.
Johnson, J.W., Oelkers, E.H., Helgeson, H.C., 1992. SUPCRT92: A software package for calculating the standard molal thermodynamic properties of minerals, gases, aqueous species, and reactions from 1 to 5000 bar and 0 to 1000 °C. Comput. Geosci. 18, 899–947. https://doi.org/10.1016/0098-3004(92)90029-Q.
Klaus, S.R., Neubauer, J., Goetz-Neunhoeffer, F., 2013. Hydration kinetics of CA_2 and CA—Investigations performed on a synthetic calcium aluminate cement. Cem. Concr. Res. 43, 62–69. https://doi.org/10.1016/j.cemconres.2012.09.005.
Kulik, D.A., Wagner, T., Dmytrieva, S.V., Kosakowski, G., Hingerl, F.F., Chudnenko, K.V., Berner, U.R., 2012. GEM-Selektor geochemical modeling package: revised algorithm and GEMS3K numerical kernel for coupled simulation codes. Comput Geosci. https://doi.org/10.1007/s10596-012-9310-6.
Langmuir, D., 1998. Aqueous environmental geochemistry.
Liu, H., Fu, Z., Yang, K., Xu, X., Bauchy, M., 2019. Machine learning for glass science and engineering: A review. J. Non-Crystalline Solids: X 4, 100036. https://doi.org/10.1016/j.nocx.2019.100036.
Lothenbach, B., Durdziński, P.T., De Weerdt, K., 2016. Thermogravimetric analysis, in: A Practical Guide to Microstructural Analysis of Cementitious Materials. Boca Raton.
Lothenbach, B., Matschei, T., Möschner, G., Glasser, F.P., 2008. Thermodynamic modelling of the effect of temperature on the hydration and porosity of Portland cement. Cem. Concr. Res. 38, 1–18. https://doi.org/10.1016/j.cemconres.2007.08.017.
Lothenbach, B., Kulik, D.A., Matschei, T., Balonis, M., Baquerizo, L., Dilnesa, B., Miron, G.D., Myers, R.J., 2019. Cemdata18: A chemical thermodynamic database for hydrated Portland cements and alkali-activated materials. Cem. Concr. Res. 115, 472–506. https://doi.org/10.1016/j.cemconres.2018.04.018.
Lothenbach, B., Winnefeld, F., 2006. Thermodynamic modelling of the hydration of Portland cement. Cem. Concr. Res. 36, 209–226. https://doi.org/10.1016/j.cemconres.2005.03.001.
Mangabhai, R.J. (Ed.), 2019. Calcium aluminate cements: proceedings of a symposium dedicated to H.G. Midgley, London, July 1990. CRC Press, Boca Raton.
Matschei, T., Lothenbach, B., Glasser, F.P., 2007. The AFm phase in Portland cement. Cem. Concr. Res. 37, 118–130. https://doi.org/10.1016/j.cemconres.2006.10.010.
Mauro, J.C., n.d. Topological constraint theory of glass. American Ceramic Society Bulletin 90, 7.
Oey, T., Kumar, A., Falzone, G., Huang, J., Kennison, S., Bauchy, M., Neithalath, N., Bullard, J.W., Sant, G., 2016. The influence of water activity on the hydration rate of tricalcium silicate. J. Am. Ceram. Soc. 99, 2481–2492. https://doi.org/10.1111/jace.14181.
Oey, T., Kumar, A., Pignatelli, I., Yu, Y., Neithalath, N., Bullard, J.W., Bauchy, M., Sant, G., 2017a. Topological controls on the dissolution kinetics of glassy aluminosilicates. J. Am. Ceram. Soc. 100, 5521–5527. https://doi.org/10.1111/jace.15122.
Oey, T., Timmons, J., Stutzman, P., Bullard, J.W., Balonis, M., Bauchy, M., Sant, G., 2017b. An improved basis for characterizing the suitability of fly ash as a cement replacement agent. J. Am. Ceram. Soc. 100, 4785–4800. https://doi.org/10.1111/jace.14974.
Oey, T., Jones, S., Bullard, J.W., Sant, G., 2020. Machine learning can predict setting behavior and strength evolution of hydrating cement systems. J. Am. Ceram. Soc. 103, 480–490. https://doi.org/10.1111/jace.16706.
Okoronkwo, M.U., Balonis, M., Katz, L., Juenger, M., Sant, G., 2018. A thermodynamics-based approach for examining the suitability of cementitious formulations for solidifying and stabilizing coal-combustion wastes. J. Environ. Manage. 217, 278–287. https://doi.org/10.1016/j.jenvman.2018.02.095.
Okoronkwo, M.U., Glasser, F.P., 2016. Stability of strätlingite in the CASH system. Mater. Struct. 49, 4305–4318. https://doi.org/10.1617/s11527-015-0789-x.
Ouyang, B., Li, Y., Song, Y., Wu, F., Yu, H., Wang, Y., Bauchy, M., Sant, G., 2020. Learning from Sparse Datasets: Predicting Concrete's Strength by Machine Learning. arXiv:2004.14407 [cond-mat].
Ouyang, B., Song, Y., Li, Y., Wu, F., Yu, H., Wang, Y., Yin, Z., Luo, X., Sant, G., Bauchy, M., 2021. Using machine learning to predict concrete's strength: learning from small datasets. Eng. Res. Express 3, 015022. https://doi.org/10.1088/2631-8695/abe344.
Pargent, F., 2019. A Benchmark Experiment on How to Encode Categorical Features in Predictive Modeling. undefined.
Paszke, A., Gross, S., Massa, F., Lerer, A., Bradbury, J., Chanan, G., Killeen, T., Lin, Z., Gimelshein, N., Antiga, L., Desmaison, A., Kopf, A., Yang, E., DeVito, Z., Raison, M., Tejani, A., Chilamkurthy, S., Steiner, B., Fang, L., Bai, J., Chintala, S., 2019. PyTorch: An Imperative Style, High-Performance Deep Learning Library, in: Advances in Neural Information Processing Systems. Curran Associates, Inc.
Piekkari, K., Ohenoja, K., Isteri, V., Tanskanen, P., Illikainen, M., 2020. Immobilization of heavy metals, selenate, and sulfate from a hazardous industrial side stream by using calcium sulfoaluminate-belite cement. J. Clean. Prod. 258, 120560 https://doi.org/10.1016/j.jclepro.2020.120560.
Pignatelli, I., Kumar, A., Bauchy, M., Sant, G., 2016. Topological Control on Silicates' Dissolution Kinetics. Langmuir 32, 4434–4439. https://doi.org/10.1021/acs.langmuir.6b00359.
Poon, C.S., Qiao, X.C., Lin, Z.S., 2003. Pozzolanic properties of reject fly ash in blended cement pastes. Cem. Concr. Res. 33, 1857–1865. https://doi.org/10.1016/s0008-8846(03)00213-8.
Poon, C.S., Qiao, X.C., Lin, Z.S., 2004. Effects of flue gas desulphurization sludge on the pozzolanic reaction of reject-fly-ash-blended cement pastes. Cem. Concr. Res. 34, 1907–1918. https://doi.org/10.1016/j.cemconres.2004.02.027.
Renew, J.E., Huang, C.-H., Burns, S.E., Carrasquillo, M., Sun, W., Ellison, K.M., 2016. Immobilization of heavy metals by solidification/stabilization of co-disposed flue gas desulfurization brine and coal fly ash. Energy Fuels 30, 5042–5051. https://doi.org/10.1021/acs.energyfuels.6b00321.
Rietveld, H.M., 1969. A profile refinement method for nuclear and magnetic structures. J Appl Crystallogr 2, 65–71. https://doi.org/10.1107/S0021889869006558.
Shi, Z., Geiker, M.R., Lothenbach, B., De Weerdt, K., Garzón, S.F., Enemark-Rasmussen, K., Skibsted, J., 2017. Friedel's salt profiles from thermogravimetric analysis and thermodynamic modelling of Portland cement-based mortars exposed to sodium chloride solution. Cem. Concr. Compos. 78, 73–83. https://doi.org/10.1016/j.cemconcomp.2017.01.002.
Song, Y., Yang, K., Chen, J., Wang, K., Sant, G., Bauchy, M., 2021a. Machine Learning Enables Rapid Screening of Reactive Fly Ashes Based on Their Network Topology. ACS Sustainable Chem. Eng. https://doi.org/10.1021/acssuschemeng.0c06978.
Song, Y., Yang, K., Chen, J., Wang, K., Sant, G., Bauchy, M., 2021b. Machine learning enables rapid screening of reactive fly ashes based on their network topology. ACS Sustainable Chem. Eng. 9, 2639–2650. https://doi.org/10.1021/acssuschemeng.0c06978.
Sorrentino, D., Sorrentino, F., George, M., 1995. Mechanisms of hydration of calcium aluminate cements. Material Science Concrete 4, 41–90.
Thoenen, T., Hummel, W., Berner, U., Curti, E., 2014. The PSINagra chemical thermodynamic database 12/07, Villigen PSI. ed. Switzerland.
Vollpracht, A., Lothenbach, B., Snellings, R., Haufe, J., 2016. The pore solution of blended cements: a review. Mater. Struct. 49, 3341–3367. https://doi.org/10.1617/s11527-015-0724-1.
Wagner, T., Kulik, D.A., Hingerl, F.F., Dmytrieva, S.V., 2012. GEM-Selektor geochemical modeling package: TSolMod library and data interface for multicomponent phase models. Can. Mineral. 50, 1173–1195. https://doi.org/10.3749/canmin.50.5.1173.
Wang, T., Ishida, T., 2019. Multiphase pozzolanic reaction model of low-calcium fly ash in cement systems. Cem. Concr. Res. 122, 274–287. https://doi.org/10.1016/j.cemconres.2019.04.015.